TRANSONIC AERODYNAMIC DESIGN EXPERIENCE

E. Bonner
Rockwell International Corporation
North American Aircraft Operations
Los Angeles, California

SUMMARY

Advancements have occurred in transonic numerical simulation that place aerodynamic performance design into a relatively well developed status. Efficient broad band operating characteristics can be reliably developed at the conceptual design level. Recent aeroelastic and separated flow simulation results indicate that systematic consideration of an increased range of design problems appears promising. This emerging capability addresses static and dynamic structural/aerodynamic coupling and nonlinearities associated with viscous dominated flows.

INTRODUCTION

Substantial advancements have occurred in transonic numerical design and analysis since the last Transonic Perspective[1] was held at the Ames Research Center in the spring of 1981. The modeling of general wing-body arrangements is well developed at the full potential/Euler level and has been coupled to boundary layer equations to approximate the effects of viscosity. The interaction of multiple surfaces can be systematically treated. In short, most of the identified deficiencies at the time[2] have been eliminated. Recently, modeling of extensively separated flows has been successfully demonstrated using Reynolds-averaged Navier-Stokes analysis. This is encouraging and provides impetus to numerically investigate increasingly complex design conditions.

One of the pacing technologies in numerical design and analysis is grid generation. The wide variety of geometry and flow gradients emphasizes multiblock/multigrid simulations in the interest of generality and computational efficiency through accelerated solution convergence. Grid size constraints places emphasis on adaptive strategies in order to resolve viscous regions, local interactions, etc.

The development of unified solution algorithms for nonlinear equations[3,4] allows consideration of subsonic (elliptic), transonic (mixed elliptic - hyperbolic) and supersonic (hyperbolic) flows for both steady and unsteady problems.

SYMBOLS

AR	Aspect Ratio
c	Local Chord
b	Wing Span
C_D	Drag Coefficient
C_L	Lift Coefficient
C_{L_α}	Theoretical Lift Curve Slope - Per Radian
C_P	Static Pressure Coefficient, $\frac{P-P_\infty}{q_\infty}$
I	Inviscid
M	Mach Number
L/D	Lift-Drag Ratio
NT	Number of Time Steps
P	Static Pressure
q	Dynamic Pressure
RANS	Reynolds-averaged Navier-Stokes
R_n	Mean Aerodynamic Chord Reynolds Number
S	Suction Parameter (see Equation 1)
SFP	Supersonic Full Potential
TWT	Rockwell Trisonic Wind Tunnel
UPWT	Langley Unitary Plan Wind Tunnel
V	Viscous
x,y,z	Axial, Lateral, Vertical Cartesian Coordinates
α	Angle of Attack
δ	Flap Deflection Angle
θ	Twist Angle
Λ	Sweep Angle

Subscripts:

F	Friction
LE	Leading Edge
t	Tip
∞	Free Stream

DISCUSSION

Representative computational simulations will be presented to illustrate the current state-of-the-art in transonic aerodynamic numerical design. Related results at subsonic and supersonic speeds will also be given since these conditions are often relevant to transonic flows vis-a-vis imposed geometric constraints.

Two specific cases will be selected for detailed discussion. The first addresses conceptual numerical design capability. The second describes the simulation generality which is possible using unified solution algorithms. The discussion is concluded by citing a number of related developments to further define the scope and success of recent transonic numerical efforts.

Advanced Concept

A multistage process is used to achieve a conceptual aerodynamic design defined here as that activity which is used to numerically screen and define the arrangement and flow characteristics prior to committing to a subscale test. The procedure is summarized on figure 1 in conjunction with the approximating equations used and proceeds from left to right. Linear theory is used to establish necessary far field thickness and lifting constrained optimums and associated geometry. A transonic nonlinear analogue is currently under development[5]. Linear results are necessary but not sufficient in nature since they do not explicitly deal with embedded shock waves and viscous effects. Full potential and Euler/boundary layer simulations are subsequently used to resolve the wave system and manage its interaction with the boundary layer. Transonic aerodynamic deficiencies can be commonly traced to a failure to deal with this consideration adequately. Finally, there is a design space in which viscous effects dominate to the extent that force and moment nonlinearities dictate structural and stability/control system requirements. These flows are typically extensively separated and are statically or dynamically coupled with the structure. Because of the complex nature of such conditions, the slowest progress from both a numerical and test standpoint has resulted for this class of problems.

In order to illustrate the process of figure 1, the following example[6] is presented for the tactical fighter concept of figure 2 which had transonic acceleration, supersonic cruise, and subsonic/transonic/supersonic maneuver design points. These diverse operating conditions were reconciled using 25 percent chord full span deflectable leading and trailing edge wing flaps to provide variable camber and an aeroelastically tailored structure to increase nose-down twist with pitch angle. Subsonic/transonic maneuver design pretest expectations in terms of wing surface pressure coefficient distributions are presented on figures 3 and 4, respectively. The secondary peaks are due to the discrete deflections of the two-element leading edge and single-element trailing edge flaps. The leading edge peak was not fully suppressed in order to reduce these local accelerations. Full potential simulation with and without boundary layer modeling indicated that trailing edge type separation would exist. At

M=0.9 a shock wave of increasing spanwise strength occurred downstream of the trailing edge flap hingeline. The flow is separated at the foot of the shock in the outboard region and is partially a consequence of supersonic efficiency considerations which limit the geometric camber between the flaps. The approach here is thus one of accepting trailing edge separation and limiting its extent through pressure gradient location. Post-test comparison with measurements presented on figures 3 and 4 indicate that this objective was realized. Surface flow data (not shown) further corroborated the anticipated separation extent.

Measured performance results in terms of the aerodynamic lifting efficiency parameter

$$S = \frac{C_L^2 / C_{L_\alpha} - (C_D - C_{DF})}{C_L^2 / C_{L_\alpha} - C_L^2 / \pi AR} \qquad (1)$$

are presented on figure 5. Two cases are shown. The first design placed increased emphasis on acceleration/cruise while the second placed increased emphasis on maneuver. Both were designed numerically. Theoretical upper bound lifting efficiency corresponds to S=1 and is associated with an elliptic span load. S=0 corresponds to the zero suction drag of a flat plate of the same gross planform. The test derived M=0.6 variation with lift coefficient indicates the onset and growth of separation at subsonic conditions. Comparison with the transonic characteristics at M=0.9 indicates the impact of the formation and strengthening of embedded shock waves and associated upper surface separation. The test results compared to upper bound levels verify that the numerical design is operating efficiently over a broad band of operating lift coefficient at both subsonic and transonic conditions. A corollary result is that numerical pressure gradient/boundary layer control through camber and twist management is an effective strategy. The impact of twist/camber variations at supersonic speeds is presented on figure 6. Also shown is the effect of transonic considerations associated with reduced leading edge sweep and increased leading edge radius, camber and twist relative to an unconstrained supersonic design. The impact of the twist/camber changes between the first and second transonic design of figure 5 were secondary at this condition and consequently not shown. Numerical pretest expectations are in good agreement with measurements in all cases.

In summary, numerical design was very effective in developing high aerodynamic efficiency for an advanced concept over a broad Mach number/lift coefficient operating envelope and was realized with a minimal number (specifically two) of test entries. The impact of computational fluid dynamics on the design effort is summarized on figure 7 which compares the present advanced concept results with representative inventory tactical aircraft of the same class. Transonic improvements are attributed to increased lifting efficiency and supersonic improvements to increased volumetric efficiency. These and similar results not presented here indicate that numerical aerodynamic performance design has progressed to a relatively mature status. Adequate prediction of transonic drag does, however, remain an area of research, particularly for conditions which have separation present.

Research Wing-Body

A series of numerical computations will now be compared to test results for the wing-body arrangement of figure 8 to illustrate the current capability to systematically simulate a wide variety of conditions encompassing subsonic, transonic, and supersonic conditions for both attached and separated flows using a unified solution algorithm[3,4] and grid topology. The analysis is equally capable of treating unsteady as well as steady flows. Only results for the latter will be presented. The geometry under consideration is undesigned and consequently the subject pertinent to aerodynamic development is how reliably are the characteristics associated with this arrangement numerically captured. This, of course, is a prerequisite to their modification through numerical design.

The multiblock six-zone H grid topology of figure 9 was used for the numerical simulation. An isometric upper half plane of the computational domain is presented in figure 9a. A typical cross-section cut is presented on figure 9b to further define the blocking and clustering. Nominally 89,000 grid points were employed (maximum available on CRAY XMP/14) for an in core simulation. Euler results[7] for six degrees angle-of-attack at M=0.9 and 1.2 are presented on figure 10 for various wing span stations and fuselage polar angle locations of $\pm 15°$ above the plane of the wing where the wing-body interaction is strong. Comparison with measured surface pressure coefficient results is excellent. At M=0.9, a strong shock exists on the fuselage above the plane of the wing. Embedded leading and trailing edge shock exists on the suction side of the wing which increase in strength spanwise until they coalesce and further increase in strength until shock-induced separation occurs very near the wing tip. The flow at M=1.2 has an upper surface trailing edge shock and is sufficiently weak that the flow is attached. All major features of the flow have been accurately forecast except, of course, the shock-induced tip separation. Ample warning was provided even in this area that the shock was strong and that separation was consequently a possibility. From a design viewpoint, it can either be accepted or explicitly dealt with through redesign. The Euler numerical results typically required 20 minutes of CRAY CPU time per case. It should be pointed out that a 33,660 grid point single zone C-H grid full potential simulation at M=0.9 produced similar prediction success in 80 CPU seconds. No important rotational flow effects consequently existed for this case. A similar conclusion at supersonic speeds is provided by the space marching full potential and Euler results of figure 6.

The multiblock grid of figure 9 was subsequently used for turbulent Navier-Stokes simulation of the research wing-body arrangement. Typical impact of angle-of-attack on measured wing surface pressure coefficient characteristics is presented on figure 11. The inboard upper surface loading increases with the leading edge suction peak exhibiting pronounced broadening which is indicative of the formation of a vortex in this region. The outboard wing exhibits a pronounced decrease in loading and a flat upper surface pressure level typical of wing stall. Clearly this is a relatively complex viscous dominated flow which provides a difficult practical test for Reynolds-averaged Navier-Stokes

simulation. Two cases were selected for evaluation -- M=0.6, α=14°, and M=0.9, α=10°, corresponding to the highest angle-of-attack tested at each Mach number. Both exhibit the previously discussed inboard vortex/outboard separation behavior.

A zero equation (Baldwin-Lomax) turbulence model was used in zones 1 and 4 of figure 9b for the viscous simulation. The numerical analysis is compared to measured surface pressure results on figures 12 and 13. The major features of the flow are well reproduced for both cases. In particular, the formation of the inboard wing vortex and the outboard wing stall are captured. Considering the relatively coarse (limited by available core) grid being used to simulate the phenomena, the results are quite good. The potential for using such analysis for structural design and high angle-of-attack viscous dominated nonlinear modeling appears promising. The Navier-Stokes solution discussed previously required between 1-1/2 to 2-1/2 CRAY CPU hours to nominally converge. Although this level of computer resources is considerable, it is not unreasonable from an aerodynamic design point of view. This is particularly true if such simulations are used discriminately and projected to advanced state-of-the-art computers such as the CRAY 2.

In summary, numerical simulation of a research wing-body arrangement was successfully demonstrated at subsonic, transonic, and supersonic speeds. Both attached and separated flow conditions were considered. These results were achieved with a unified solution algorithm and multizone grid topology. The associated computer resources were consistent with advanced concept development activities. The viscous modeling success indicates that systematic consideration of strong viscous interaction design problems appears promising.

Related Advancements

Finally, a series of developments will be cited to further define the scope and success of recent transonic numerical efforts. Table I summarizes these activities. Detailed results are provided in the indicated references and will not be repeated here for brevity. Examination of the analyses and comparison with test measurements where pertinent establish that advancement is occurring in a variety of areas covering grid generation, multiple surface interactions, steady and unsteady aeroelasticity, and strongly shocked and separated flows. This research considered a hierarchy of fluid dynamic equations covering full potential, Euler, and Reynolds-averaged Navier-Stokes approximations. Unification of the grid topology and flow solvers is being emphasized in order to reduce the effort associated with development of simulations covering a wide design space.

CONCLUDING REMARKS

Substantial progress has occurred in transonic numerical simulation and design since the last Transonic Perspective. Aerodynamic numerical performance design is in a relatively well developed state as evidenced by the ability to reliably develop efficient broad band characteristics at the conceptual design level. Recent aeroelastic and separated flow simulation results indicate that a capability to consider an important new range of design problems is emerging. Grid generation remains a pacing technology for numerical aerodynamic design efforts. It becomes increasingly demanding for complex geometry/viscous flow resolution. Overall grid size limits must be compatible with conceptual development activity in terms of time and resources available if advanced numerical analyses are to have the desired early design impact.

REFERENCES

1. Transonic Aerodynamics, Progress in Astronautics and Aeronautics, Volume 81, David Nixon Editor, 1981

2. IBID, chapter X

3. Shankar, V., and Chakravarthy, S., "Development and Application of Unified Algorithms for Problems in Computational Science," NASA CP-2454 Supercomputing in Aerospace Sciences Symposium Proceedings, pp. 87-107, Ames Research Center, March 10-12, 1987

4. Chakravarthy, S. and Szema, K. Y., "Advances in Finite Difference Techniques for Computational Fluid Dynamics," Chapter in State of the Art Survey in Computational Mechanics, edited by A. K. Noor and J. T. Oden, to be published by ASME, April 1988

5. Malmuth, N. D., and Cole, J. D., "Wave Drag Due to Lift for Transonic Airplanes," NASA CP3020, 1989

6. Bonner, E., "Nonlinear Aerodynamic Wing Design," NASA CR 3950, December 1985

7. Woan, C. J., and Chakravarthy, S. R., "Transonic Euler Calculation of a Wing-Body Configuration Using a High Accuracy TVD Scheme," Proposed Paper AIAA 6th Applied Aerodynamics Conference, June 6-8, 1988

TABLE I

ADDITIONAL TRANSONIC SIMULATION RESULTS

Simulation	Formulation	Reference
Grid Generation	Multiblock	AIAA 88-0312 88-0521
Multiple Surface Interactions	Full Potential	AIAA 86-1795
Wing-Body Static Elasticity	Full Potential	AIAA 87-0707
Wing-Body Dynamic Elasticity	Full Potential	AIAA 87-1238
Subcritical, Critical & Supercritical Inlet Flow	Euler	Unpublished
Boattail, Ramp, & Back Step Separation	Reynolds-averaged Navier-Stokes	NASA CP-2454 pp. 87-107
Attached & Separated Nozzle Flow	Reynolds-averaged Navier-Stokes	Proposed Paper AIAA 6th Applied Aerodynamic Conference, June 1988
Cavity Flow	Reynolds-averaged Navier-Stokes	AIAA 87-0117
Attached & Separated Duct Flow	Reynolds-averaged Navier-Stokes	Unpublished

SYMBOLS

AR	Aspect Ratio
c	Local Chord
b	Wing Span
C_D	Drag Coefficient
C_L	Lift Coefficient
C_{L_α}	Theoretical Lift Curve Slope - Per Radian
C_P	Static Pressure Coefficient, $\frac{P-P_\infty}{q_\infty}$
I	Inviscid
M	Mach Number
L/D	Lift-Drag Ratio
NT	Number of Time Steps
P	Static Pressure
q	Dynamic Pressure
RANS	Reynolds-averaged Navier-Stokes
R_n	Mean Aerodynamic Chord Reynolds Number
S	Suction Parameter (see Equation 1)
SFP	Supersonic Full Potential
TWT	Rockwell Trisonic Wind Tunnel
UPWT	Langley Unitary Plan Wind Tunnel
V	Viscous
x,y,z	Axial, Lateral, Vertical Cartesian Coordinates
α	Angle of Attack
δ	Flap Deflection Angle
θ	Twist Angle
Λ	Sweep Angle

Subscripts:

F	Friction
LE	Leading Edge
t	Tip
∞	Free Stream

TABLE I

ADDITIONAL TRANSONIC SIMULATION RESULTS

Simulation	Formulation	Reference
Grid Generation	Multiblock	AIAA 88-0312 88-0521
Multiple Surface Interactions	Full Potential	AIAA 86-1795
Wing-Body Static Elasticity	Full Potential	AIAA 87-0707
Wing-Body Dynamic Elasticity	Full Potential	AIAA 87-1238
Subcritical, Critical & Supercritical Inlet Flow	Euler	Unpublished
Boattail, Ramp, & Back Step Separation	Reynolds-averaged Navier-Stokes	NASA CP-2454 pp. 87-107
Attached & Separated Nozzle Flow	Reynolds-averaged Navier-Stokes	Proposed Paper AIAA 6th Applied Aerodynamic Conference, June 1988
Cavity Flow	Reynolds-averaged Navier-Stokes	AIAA 87-0117
Attached & Separated Duct Flow	Reynolds-averaged Navier-Stokes	Unpublished

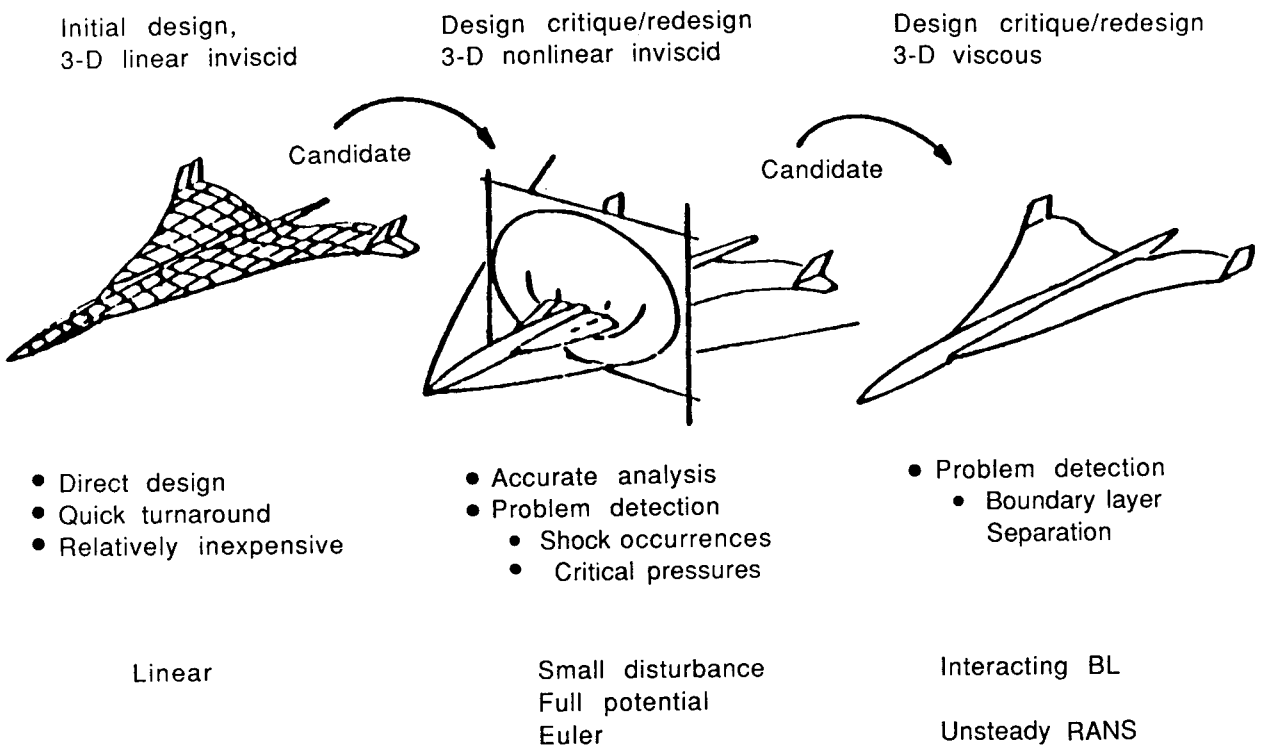

Figure 1. Numerical Design Approach

GEOMETRIC PARAMETER	WING (TRAP)	VERTICAL (TRAP)
ASPECT RATIO	3	1
TAPER RATIO	0.2	0.2
LE SWEEP	48°	55°
DIHEDRAL	0	70°
THICKNESS RATIO	0.04	0.04

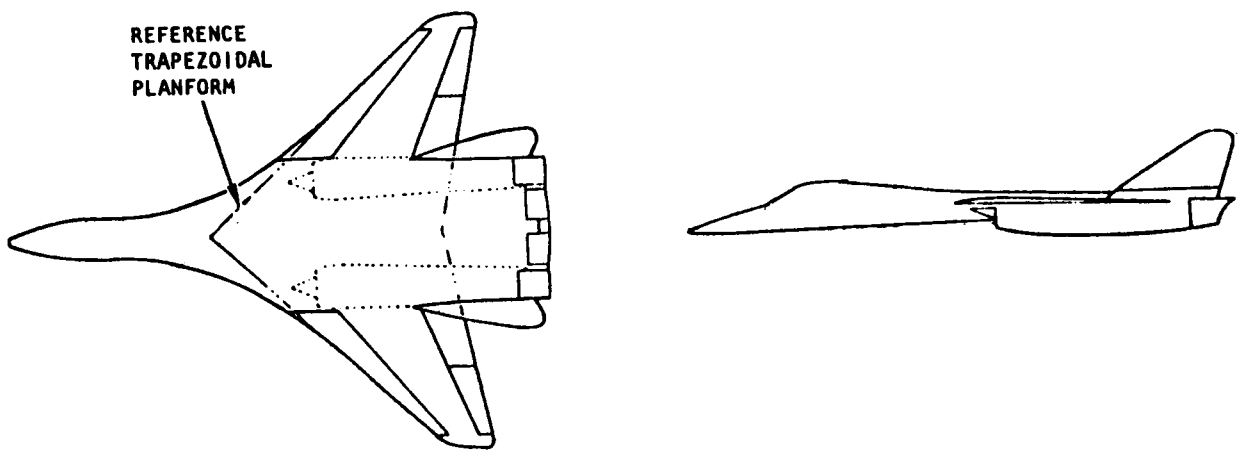

Figure 2. **Advanced Concept**

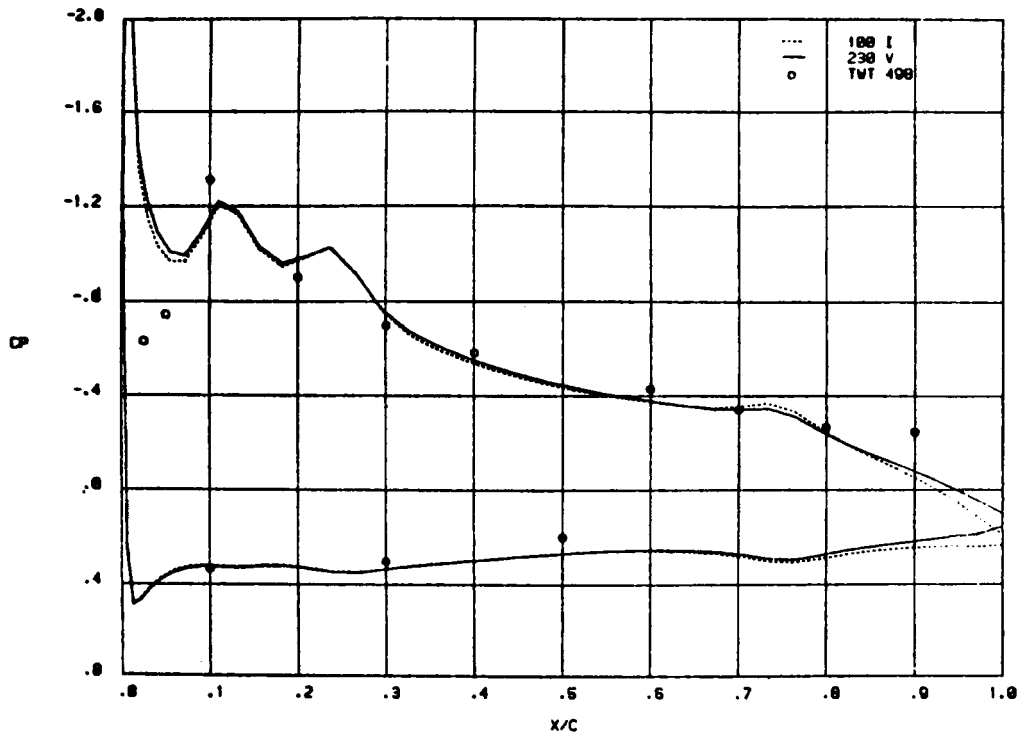

(a) 2Y/b = 0.4

Figure 3. Advanced Concept Subsonic Wing Pressure Distributions At M = 0.6, α = 14°, Rn = 5 x 10^6

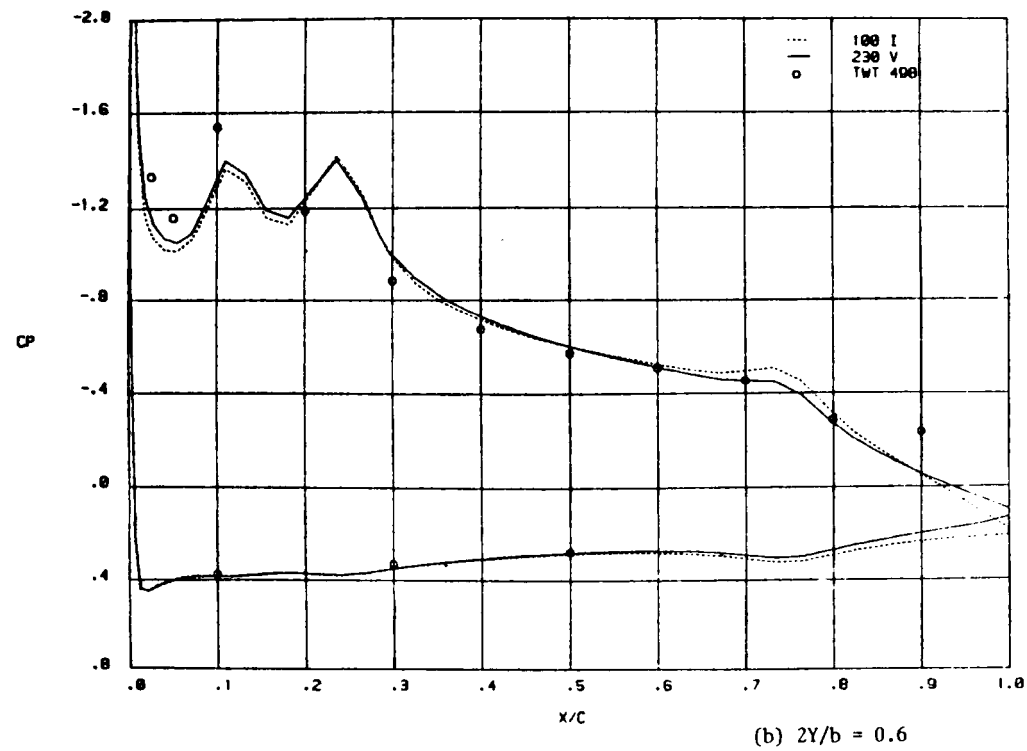

(b) 2Y/b = 0.6

Figure 3. Continued

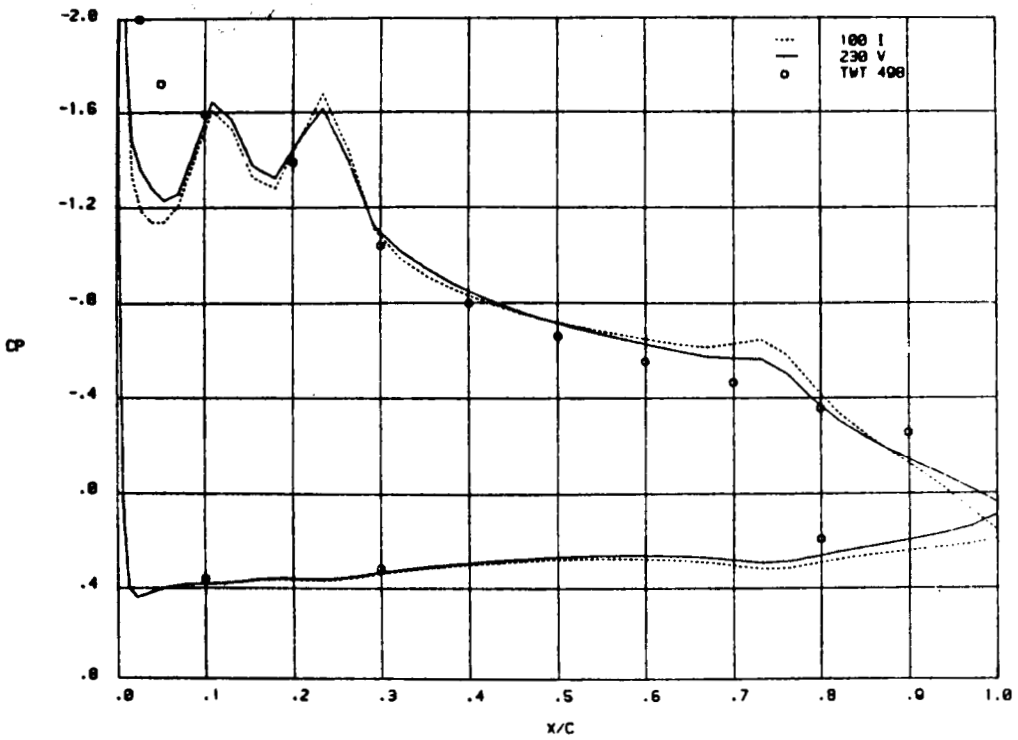

(c) 2Y/b = 0.8

Figure 3. Concluded

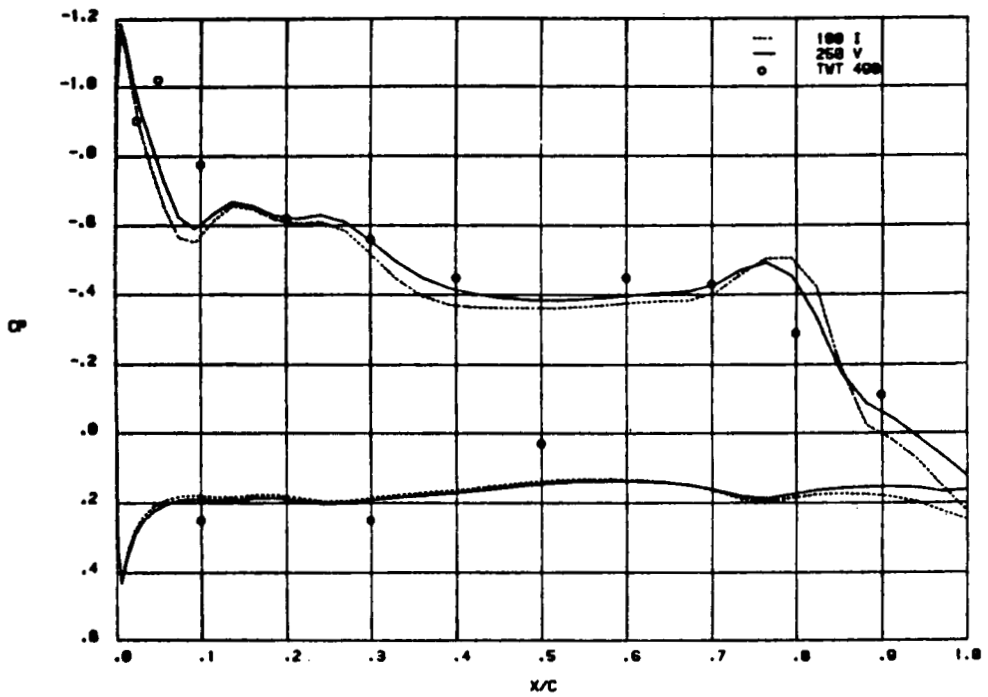

(a) 2Y/b = 0.4

Figure 4. Advanced Concept Transonic Wing Pressure Distributions At M = 0.9, α = 8.25°, Rn = 5 x 10^6

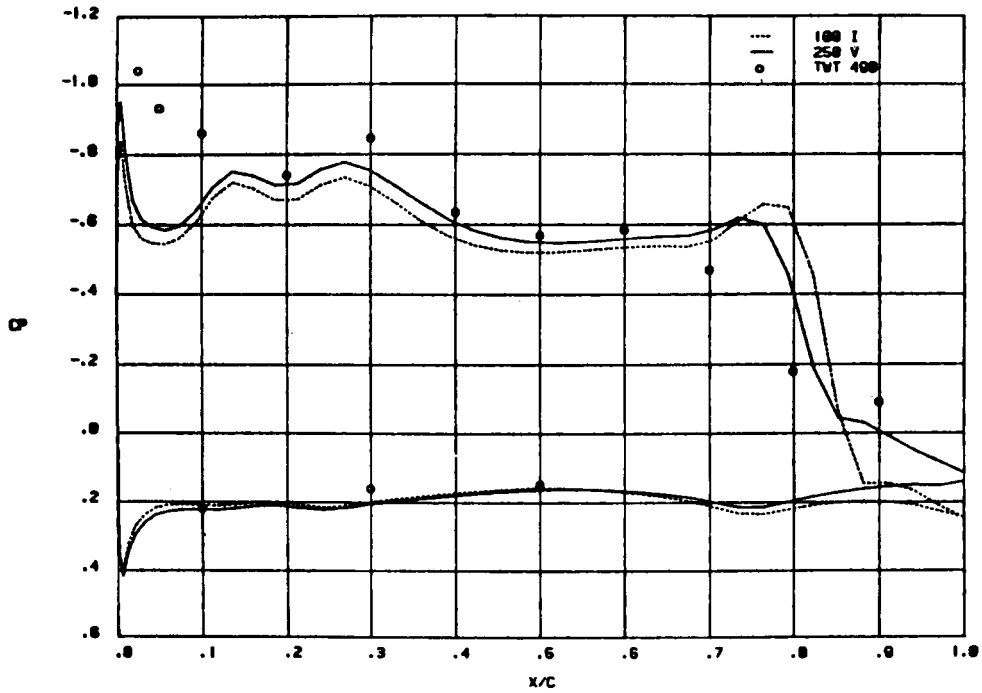

(b) 2Y/b = 0.6

Figure 4. Continued

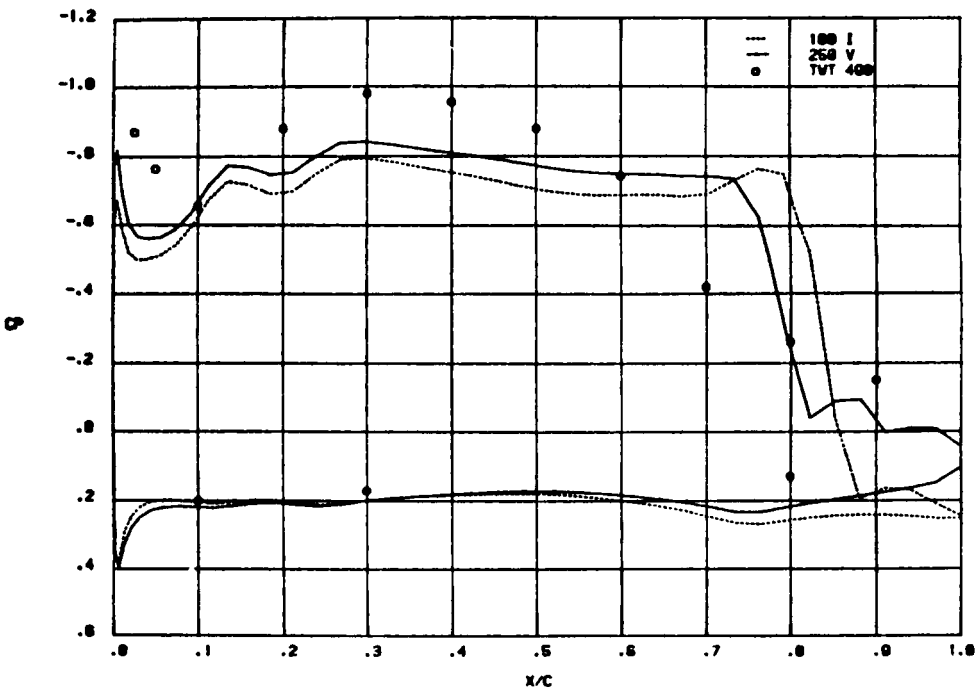

(c) 2Y/b = 0.8

Figure 4. Concluded

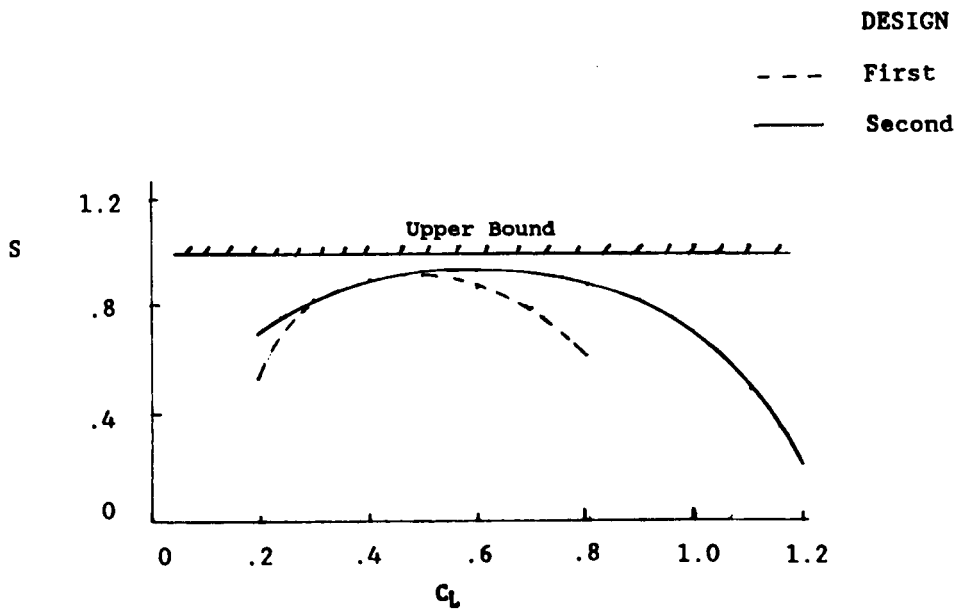

a) M = 0.6

Figure 5. Advanced Concept Test Derived Subsonic/Transonic Lifting Efficiency

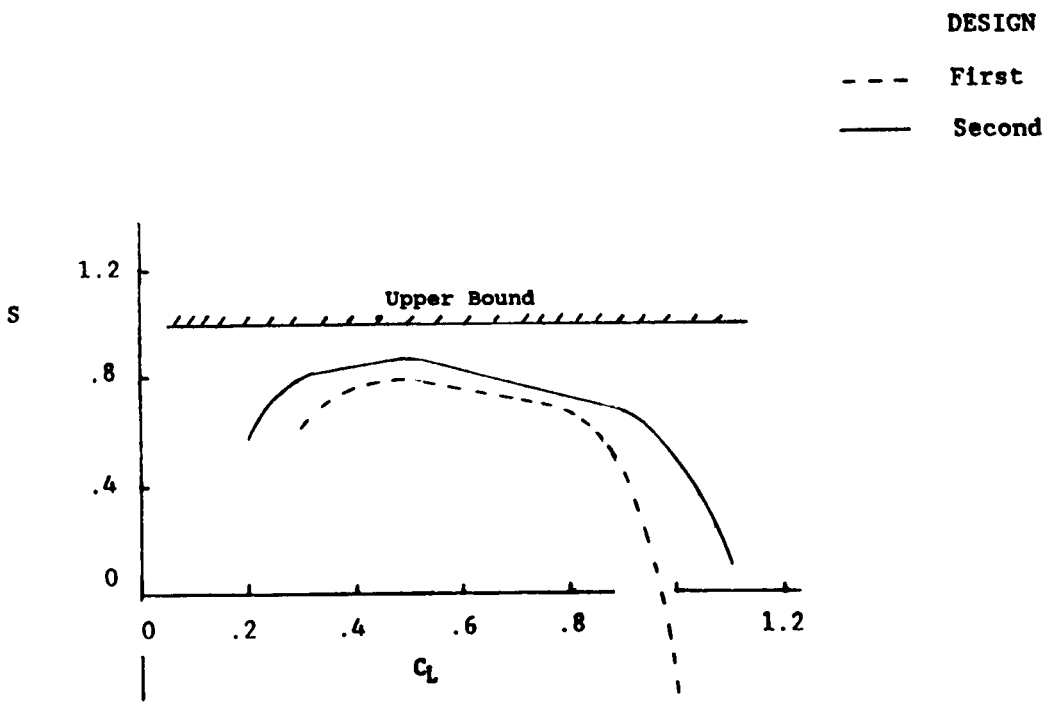

b) M = 0.9

Figure 5. Concluded

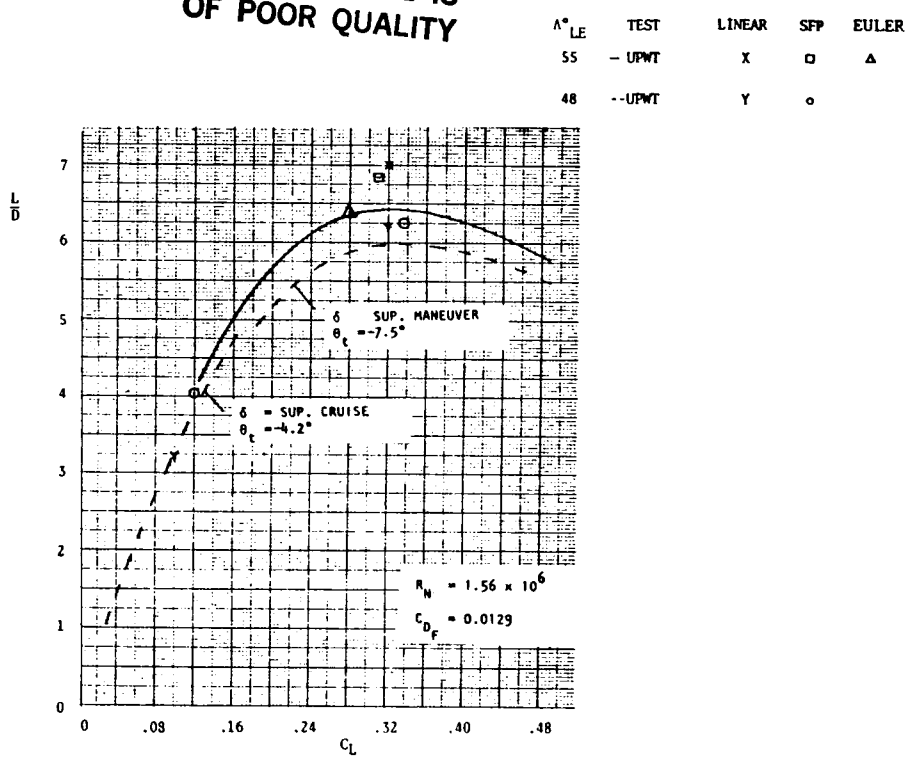

Figure 6. Avanced Concept Measured and Predicted Aerodynamic Efficiency At M=1.6

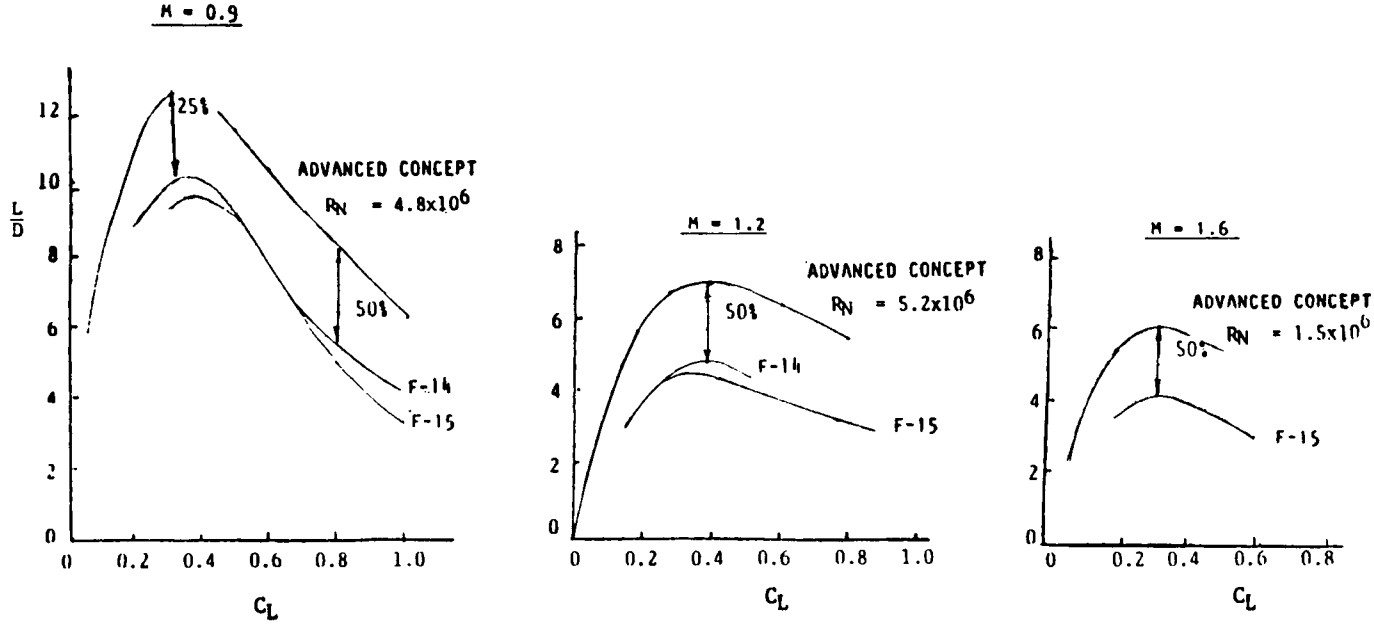

Figure 7. Impact of Numerical Design On Aerodynamic Development

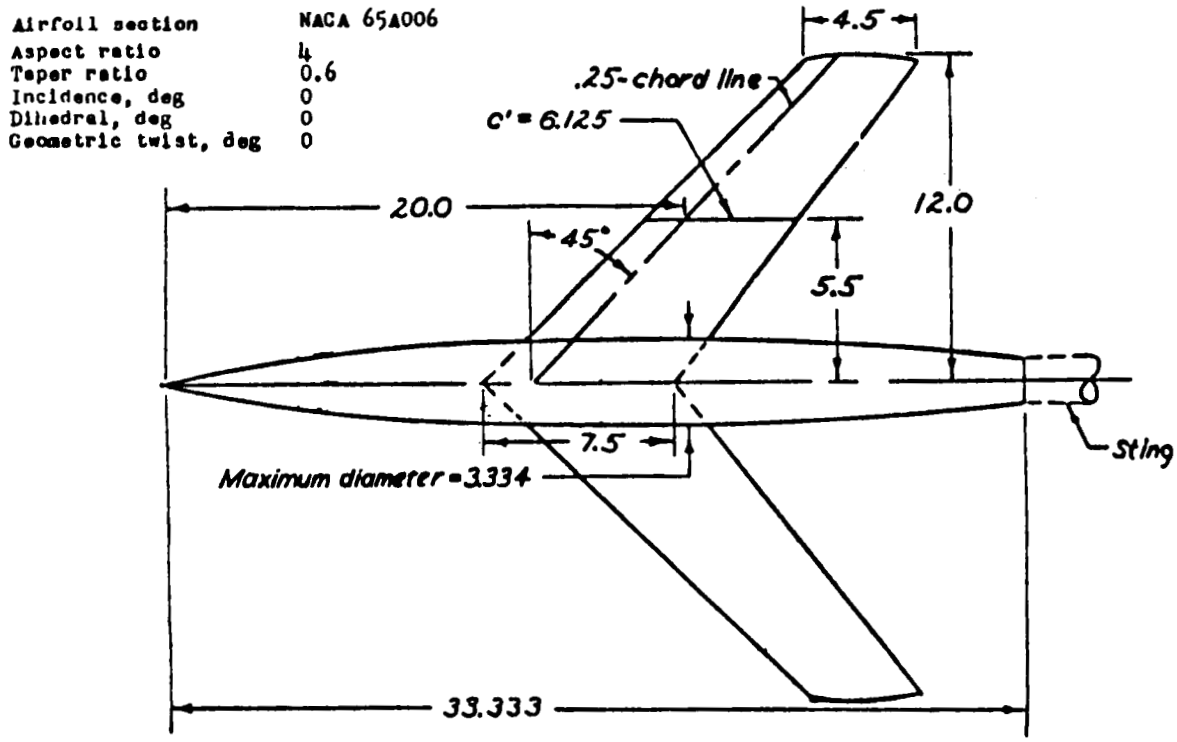

Figure 8. NACA RM L51F07 Research Wing Body

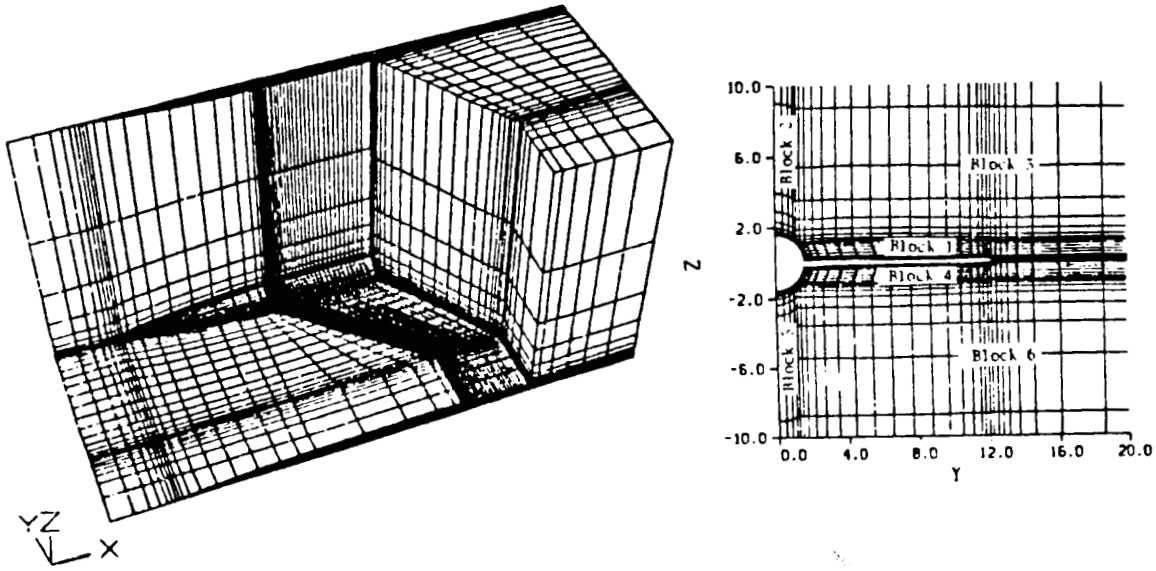

a) Isometric

b) Crossection

Figure 9. Research Wing-Body Multiblock Computational Grid

ORIGINAL PAGE IS
OF POOR QUALITY

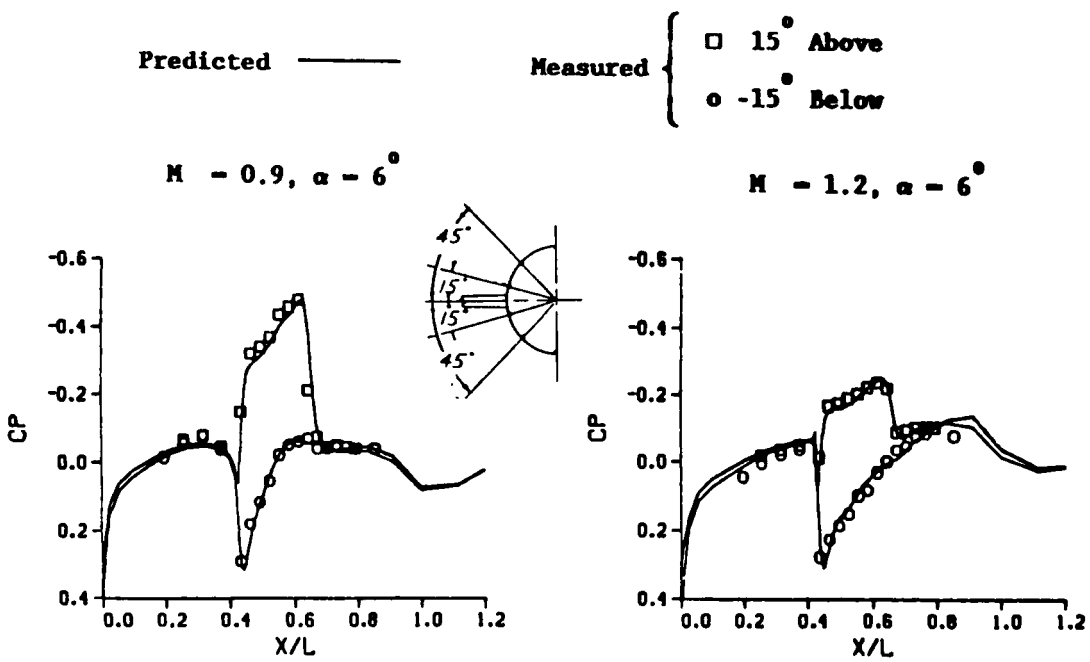

a) Fuselage , $\theta = \pm 15°$

Figure 10. Research Wing-Body Unified TVD Euler Solution at Transonic and Supersonic Conditions

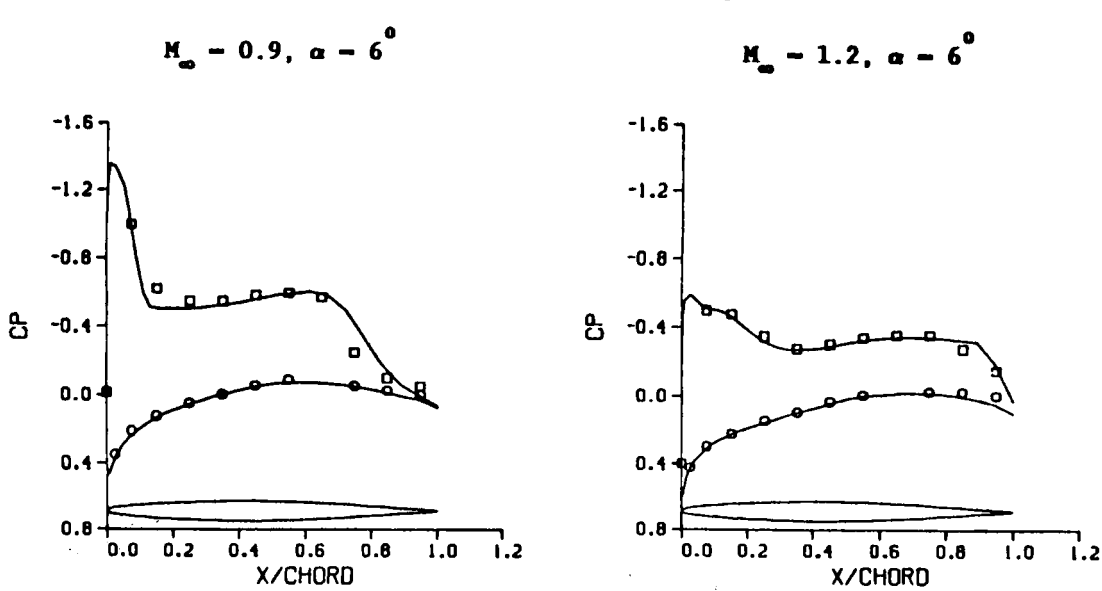

b) Wing , $2y/b = 0.4$

Figure 10. Continued

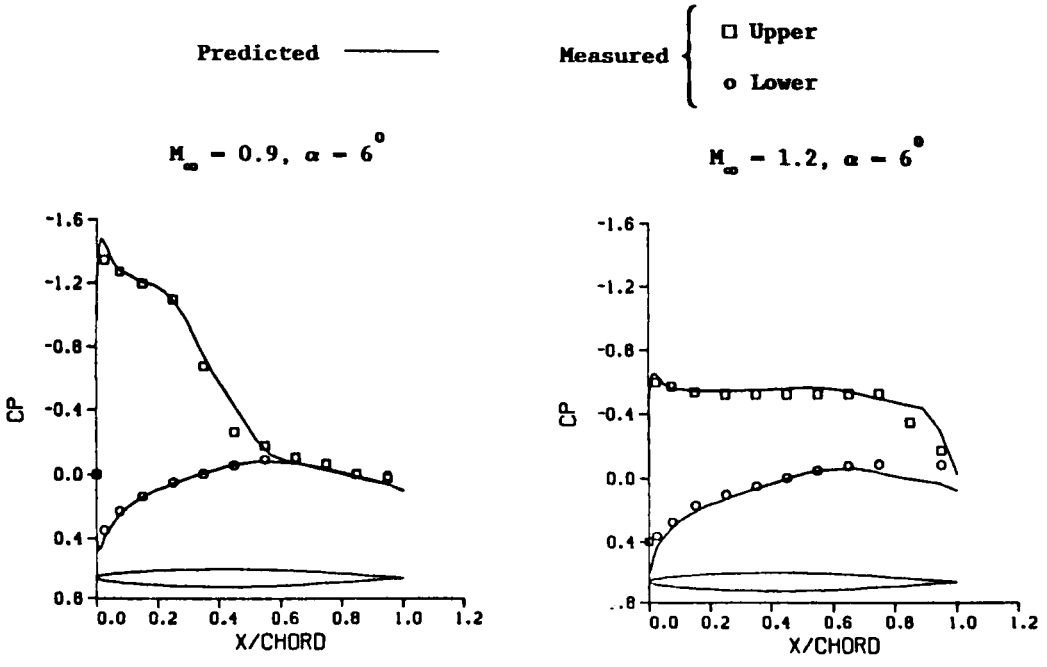

c) Wing , 2y/b = 0.8

Figure 10. Continued

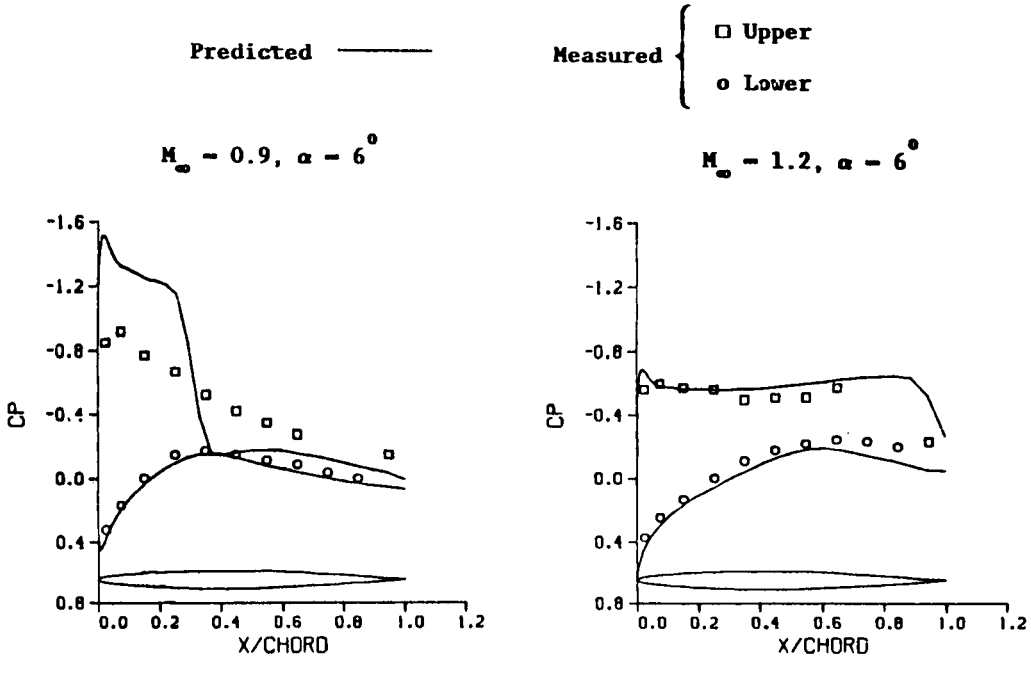

d) Wing ,2y/b = 0.95

Figure 10. Concluded

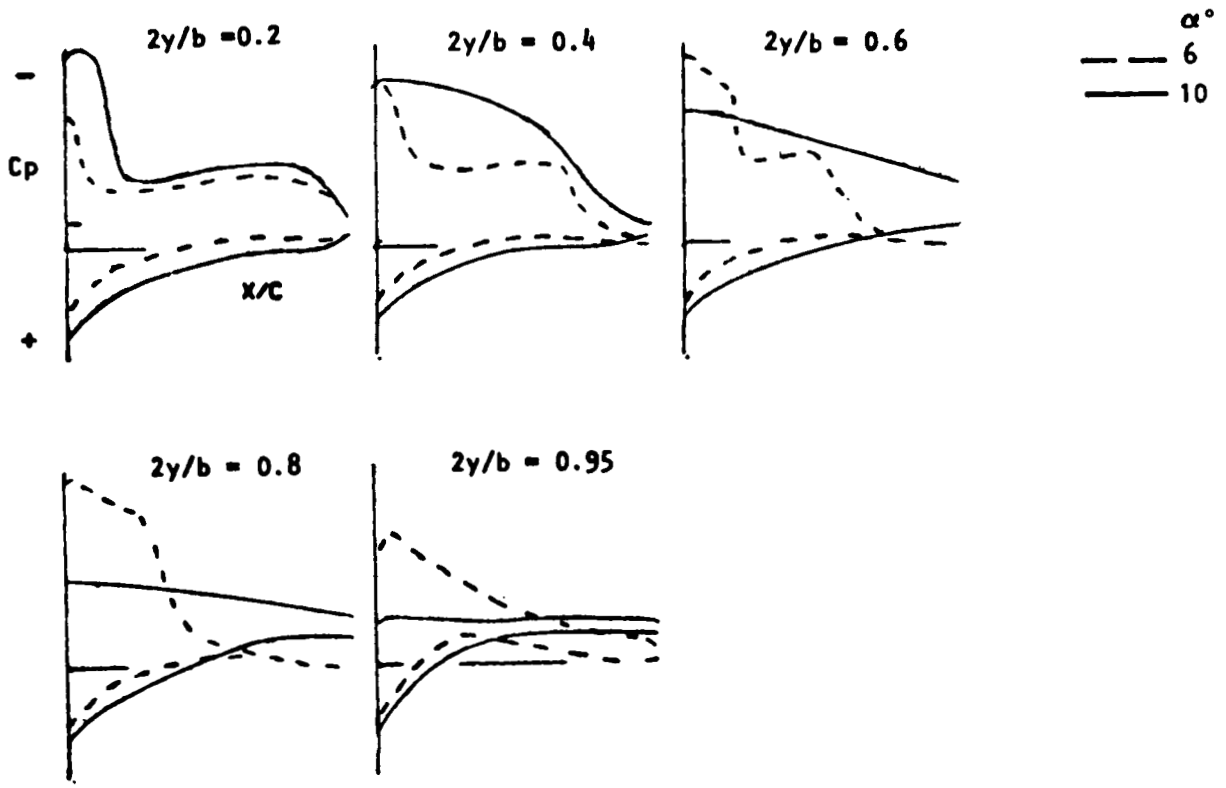

Figure 11. Effect of Viscosity on Measured Surface Pressure Characteristics for Research Wing-Body

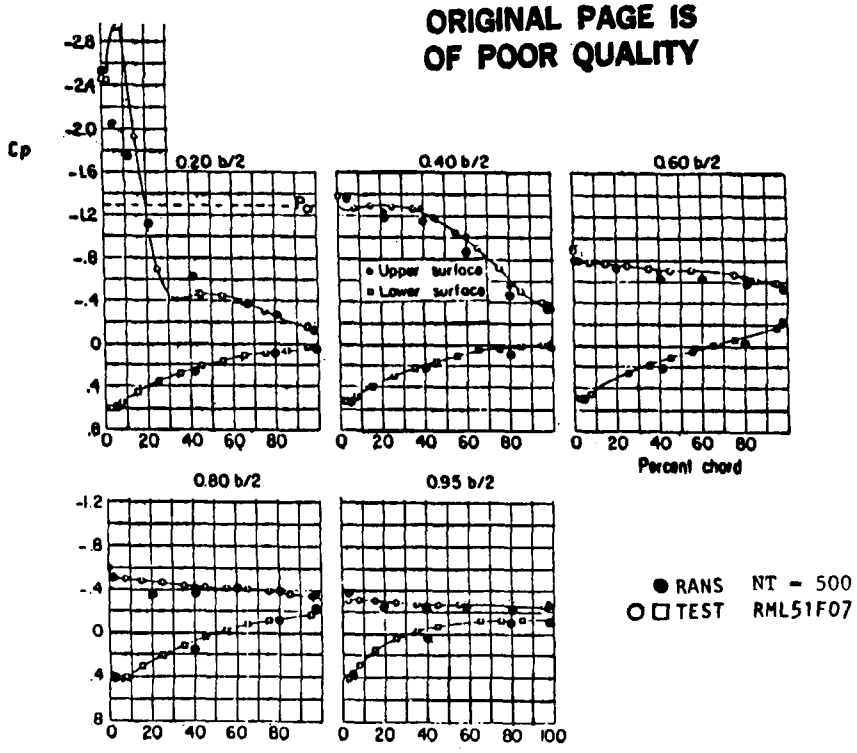

Figure 12. Reynolds Averaged Navier Stokes Separated Flow Simulation for Research Wing-Body at M = 0.6, α = 14°, Rn = 1.74 x 10^6

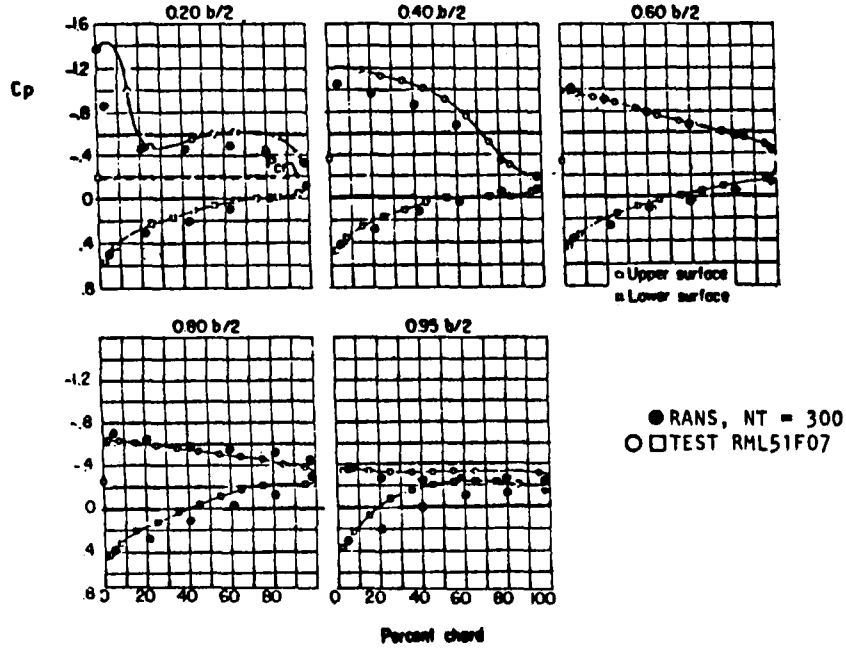

Figure 13. Reynolds Averaged Navier Stokes Separated Flow Simulation for Research Wing-Body at M = 0.9, α = 10°, Rn = 2.1 x 10^6